

Radio Halos From Simulations And Hadronic Models II: The Scaling Relations of Radio Halos

J. Donnert^{1,2,*}, K. Dolag¹, R. Cassano², G. Brunetti²

*1*Max Planck Institute for Astrophysics, P.O. Box 1317, D-85741 Garching, Germany

*2*INAF Istituto di Radioastronomia, via P. Gobetti 101, I-40129 Bologna, Italy

Accepted ???. Received ???; in original form ???

ABSTRACT

We use results from a constrained, cosmological MHD simulation of the Local Universe to predict radio haloes and their evolution for a volume limited set of galaxy clusters and compare to current observations. The simulated magnetic field inside the clusters is a result of turbulent amplification within them, with the magnetic seed originating from star-burst driven, galactic outflows. We evaluate three models, where we choose different normalisations for the cosmic ray proton population within clusters. Similar to our previous analysis of the Coma cluster (Donnert et al. 2010), the radial profile and the morphological properties of observed radio halos can not be reproduced, even with a radially increasing energy fraction within the cosmic ray proton population. Scaling relations between X-ray luminosity and radio power can be reproduced by all models, however all models fail in the prediction of clusters with no radio emission. Also the evolutionary tracks of our largest clusters in all models fail to reproduce the observed bi-modality in radio luminosity. This provides additional evidence that the framework of hadronic, secondary models is disfavored to reproduce the large scale diffuse radio emission of galaxy clusters. We also provide predictions for the unavoidable emission of γ -rays from the hadronic models for the full cluster set. None of such secondary models is yet excluded by the observed limits in γ -ray emission, emphasizing that large scale diffuse radio emission is a powerful tool to constrain the amount of cosmic ray protons in galaxy clusters.

Key words: galaxies:clusters

1 INTRODUCTION

The thermal gas, that is the dominant component in the Inter-Galactic-Medium (IGM), is mixed with magnetic fields and relativistic particles, as proven by radio observations which detected Mpc-sized diffuse radio emission from the IGM, in the form of radio halos and relics (e.g. Feretti 2003; Ferrari et al. 2008). These Mpc-scale radio sources are found in a fraction of massive clusters with complex dynamics, which suggests a connection between non-thermal emission and cluster mergers (e.g. Buote 2001; Venturi et al. 2008; Brunetti et al. 2009). Cluster mergers are the most energetic events in the universe and a fraction of the energy dissipated during these mergers may be channelled into the amplification of the magnetic fields (e.g. Dolag et al. 2002; Subramanian et al. 2006; Ryu et al. 2008) and into the acceleration of relativistic, primary, electrons and protons via shocks and turbulence (e.g. Ensslin et al. 1998; Sarazin 1999; Brunetti et al. 2001, 2004; Petrosian 2001; Gabici & Blasi 2003; Ryu et al. 2003; Cassano & Brunetti

2005; Pfrommer et al. 2006; Brunetti & Lazarian 2007; Vazza et al. 2009)

Relativistic protons in the IGM have long life-times and remain confined within galaxy clusters for a Hubble time (e.g. Völk et al. 1996; Berezhinsky et al. 1997). As a consequence they are expected to be the dominant non-thermal particle component. Collisions between these relativistic protons and the thermal protons in the IGM generate secondary particles that combined with the primary relativistic particles are expected to produce a complex emission spectrum from radio to γ -rays (e.g. Blasi 2001; Brunetti et al. 2009). Only upper limits to the γ -ray emission from galaxy clusters have been obtained so far (Reimer et al. 2003; Perkins & the VERITAS Collaboration 2006; Aharonian 2009b,a; The MAGIC Collaboration & Aleksić 2009) however the FERMI Gamma-ray telescope will shortly allow a step forward, having a chance to obtain first detections of galaxy clusters or to put stringent constraints on the energy density of the relativistic protons. Most importantly, in a few years the Low Frequency Array (LOFAR) and the Long Wavelength Array (LWA) will observe galaxy clusters at low radio frequencies with the potential to discover the bulk of the

* jdonnert@mpa-garching.mpg.de

cluster-scale synchrotron emission in the Universe (e.g. Enßlin & Röttgering 2002; Cassano et al. 2009, 2006).

The emerging theoretical picture is very complex and modern numerical simulations provide an efficient way to obtain detailed models of non thermal emission from galaxy clusters to compare with present and future observations. Advances in this respect have been recently obtained by including aspects of cosmic-ray physics into cosmological Lagrangian simulations mostly focussing on the acceleration of relativistic particles at shocks and on the relative production of secondary electrons (e.g. Pfrommer et al. 2008). In this work we investigate the non-thermal emission from secondary particles in galaxy clusters extracted from Lagrangian cosmological simulations and, for the first time, we report on an adequate comparison between our expectations and observations.

2 SIMULATIONS

The simulation was done using the cosmological simulation code GADGET-2 (Springel 2005) with a treatment for magnetic fields. It features an entropy conserving formulation of Smooth Particle Hydrodynamics (SPH) (Springel & Hernquist 2002), which is supplemented with the formulation of ideal MHD presented in Dolag & Stasyszyn (2008). The implementation follows the induction equation and computes the back reaction of the magnetic field using a symmetric formulation of the Lorentz force. We used a divergence cleaning scheme presented in Børve et al. (2001), which reduces numerical noise in shocks by subtracting the magnetic force which is proportional to the divergence of the field. It also helps to suppress the clumping instability particle based MHD codes encounter in regions with small plasma β (i.e. where magnetic pressure considerably exceeds thermal pressure).

In non radiative simulations like ours, regions with small plasma β are rare. Only the strong shocks in cores of galaxy clusters during major mergers produce enough compression to amplify the field to become dynamically dominant. These mergers are relatively brief events and are handled more accurately with our new numerical treatment (see Dolag & Stasyszyn 2008, for details). Borgani et al. (2006) have shown that non radiative simulations overpredict the gas density in cores of galaxy clusters. This affects our simulation as well and can be seen in density and magnetic field profiles as well as in X-ray luminosities. As cosmological MHD SPH simulations lack physical dissipation, radiative SPH MHD simulations are not feasible at the moment. On the other hand secondary models have difficulties reproducing the outer parts of radio halos correctly. Therefore our main focus lies on these regions, where the simulations are not affected by the overpredicted gas density.

2.1 Initial Conditions

We used a constrained realisation of the local universe (see Dolag et al. (2005) and references therein). The initial conditions are similar to those used in Mathis et al. (2002) to study the formation of the local galaxy population. They were obtained based on the IRAS 1.2-Jy galaxy survey. Its density field was smoothed on a scale of 7 Mpc, evolved back in time to $z = 50$ using the Zeldovich approximation and assumed to be Gaussian (Hoffman & Ribak 1991). The IRAS observations constrain a volume of ≈ 115 Mpc centered on the Milky Way. It was sampled with dark matter particles and embedded in a periodic box of ≈ 343 Mpc comoving. Outside of the inner region, the box is filled with dark matter particles with 1/6th

of the resolution, to cover for long range gravitational tidal forces arising from the low-frequency constrains.

In the evolved density field, many locally observed galaxy clusters can be identified by position and mass. Especially the Coma cluster (see Donnert et al. 2010) shows remarkable similarities in morphology. A fly-through of the simulation can be downloaded from the MPA Website¹.

The initial conditions were extended to include gas by splitting dark matter particles in the high resolution region into gas and dark matter particles of masses $0.69 \times 10^9 M_{\odot}$ and $4.4 \times 10^9 M_{\odot}$ respectively. Therefore the biggest clusters are resolved by about a million particles. The gravitational softening length was set to 10 kpc. This is comparable to the inter-particle separation found in the centre of the largest clusters.

2.2 Magnetic Fields from Galactic Outflows

The origins of magnetic fields in galaxy clusters are still under debate. It is assumed that some kind of early seed magnetic field is amplified by structure formation through adiabatic compression, turbulence and shear flows to values observed today ($\approx 1 - 10 \mu\text{G}$ in clusters). Three main classes of models for the seed field exist: At first the seed fields can be created in shocks through the "Biermann battery" (Kulsrud et al. 1997; Ryu et al. 1998; Miniati et al. 2001). A second class of models invokes primordial processes to predict seed fields that fill the entire volume of the universe. The coherence length of these fields strongly depends on the details of the model (see Grasso & Rubinstein 2001, for a review). Finally the seed can be produced by AGN (Enßlin et al. 1997; Furlanetto & Loeb 2001) or starbursting galaxies (Völk & Atoyan 2000) at high redshift ($z \approx 4 - 6$), whose outflows contaminate the proto-cluster region.

Cosmological simulations using SPH (Dolag et al. 1999, 2002, 2005) and grid based Adaptive Mesh Refinement (AMR) codes (Brüggen et al. 2005; Dubois & Teyssier 2008; Li et al. 2008) were able to show that observed Faraday rotations are compatible with a cosmological seed field of $\approx 10^{-11}$ G. They also suggest that spatial distribution and structure of cluster magnetic fields are determined by the dynamics in the velocity field caused by structure formation (Dolag et al. 1999, 2002).

For this work we follow Donnert et al. (2008) in terms of magnetic field origin. They use a semianalytic model for galactic winds (Bertone et al. 2006) to seed magnetic fields in a constrained cosmological MHD SPH simulation. The continuous seeding process is approximated with an instantaneous seed at $z \approx 4$. As they were able to show, the main properties of magnetic fields obtained in clusters were not influenced by that approximation.

The wind model used assumes adiabatic expansion of a spherical gas bubble with homogeneous magnetic energy density around every galaxy below a certain mass threshold. The magnetic bubble can be characterised by radius and field strength. The galaxy injects gas into the bubble carrying frozen-in magnetic field from the disc into the bubble over the star-burst timescale. Its final size is determined by the wind velocity, which is a function of the star formation rate and the properties of the ISM. Bertone et al. (2006) give an evolution equation for the magnetic energy in the bubble depending on the star-burst timescale. The energy is converted into a dipole moment and seeded once at a chosen redshift. The magnetic

¹ http://www.mpa-garching.mpg.de/galform/data_vis/index.shtml#movie12

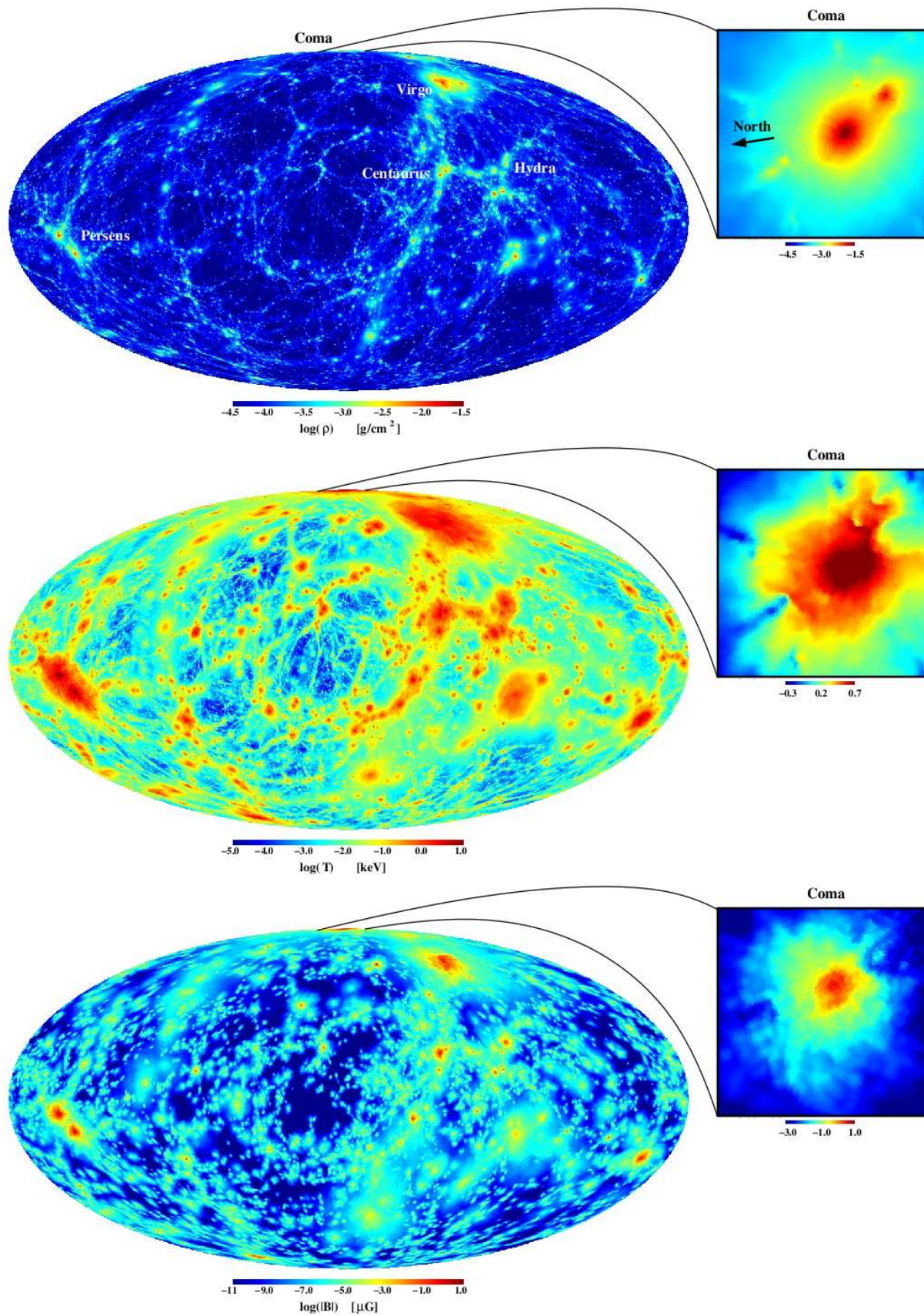


Figure 1. Full sky maps of the simulation in galactic coordinates. From top to bottom, electron density, temperature and magnetic field, projected through the whole box. The inlay shows a zoom onto a 3×3 degree region around the Coma cluster, respectively. In the upper most map, the most prominent clusters of the local universe are labeled and the arrow in the inlay points towards north.

Parameter	Value	Source
R_0	400 pc	(Klein et al. 1988)
B_0	5 μG	(Donnert et al. 2008)
B_G	3 μG	(Donnert et al. 2008)
\dot{M}_*	10 M_\odot/yr	(de Grijs 2001)
t_{sb}	150 Myr	(de Grijs 2001)
M_{ISM}	$< 300 \times 10^{12} M_\odot$	from simulation

Table 1. Summary of the parameters used for the wind model. This corresponds to the *0.1 Dipole* simulation in (Donnert et al. 2008), which fits best to observations of Faraday rotation

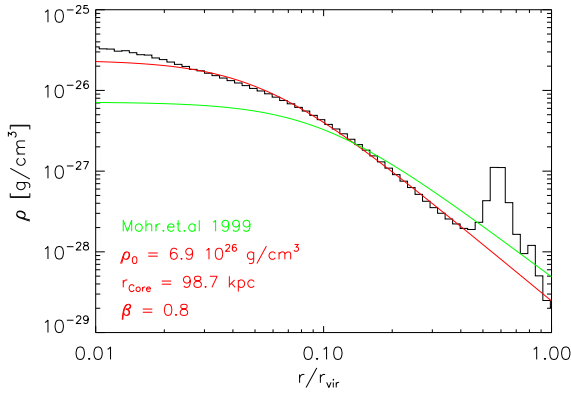


Figure 2. Radial profile of the density in our simulated Coma cluster. In red we plot the best fit beta model ($\rho_0 = 6.4 \times 10^{15}$, $\beta = 0.8$, $r_{\text{core}} = 0.06$), excluding the density bump at $0.6 R_{\text{vir}}$. A fit to observations of Coma by Mohr et al. (1999) is shown in green. Due to the non-radiativity of our simulation the gas density is overestimated by a factor of 5 in the center

field is then amplified by structure formation to μG level. For details on the wind model refer to Bertone et al. (2006); Donnert et al. (2008). Figure 1 shows full sky maps produced from the simulation, projecting the electron density, temperature and the magnetic field. The magnetic field closely follows the density distribution. The magnetic field is more patchy in the filaments compared to a cosmological seed because the seeding by individual galaxies does not overlap.

The simulation used in this work is based on the *0.1 Dipole* parameter set from Donnert et al. (2008), shown in table 1. It represents the best fit to observations of Faraday rotation presented in Donnert et al. (2008). There the parameter space was explored based on observations from the wind in M82. It was demonstrated that the resulting magnetic field does not critically depend on the exact choice of the parameters.

3 MODELLING HADRONIC SECONDARY ELECTRONS IN CLUSTERS

In secondary models proposed for the origin of radio halos (Denison 1980; Blasi & Colafrancesco 1999), the emitting cosmic ray electrons (CRE) are a product of cosmic ray proton collisions (CRp) with thermal protons in the cluster. Possible mechanisms for the injection of CRp in the IGM include shock waves caused by cluster accretion and mergers (e.g. Gabici & Blasi 2003; Ryu et al. 2003; Pfrommer et al. 2006; Vazza et al. 2009) outflows from radio galax-

ies (AGN) (e.g. Ensslin et al. 1998; Rachen 2008) and supernova driven winds (Völk et al. 1996). The resulting CRp spectrum from these theoretical scenarios is a power law (e.g. Schlickeiser 2002), that is also consistent with observations of galactic cosmic rays.

We assume a power law spectrum of CRp in the IGM and calculate the spectrum of high-energy secondary electrons under stationary conditions by considering only synchrotron and inverse Compton losses and by neglecting re-acceleration processes in the IGM (Section 3.1).

Throughout the first two of our models, we use the magnetic fields obtained from the constrained cosmological simulation described in section 2.2. In a third model we increased the magnetic field, especially at larger distances to the center, by up-scaling the magnetic field in our simulation to be $B \propto \sqrt{\rho}$, which allows for better comparison with results obtained in previous literature, as there such a relation is often used (as for example in Pfrommer et al. (2008)).

3.1 Synchrotron emission from secondary models

We consider a spectral distribution of the population of relativistic CRp described by a power law in energy E_p :

$$N(E_p) = K_p E_p^{-\alpha_p}; \quad (1)$$

if not stated otherwise, we use a spectral index $\alpha_p = 2.6$. The normalisation K_p is model dependent and is defined in the next Sections.

The main channel of hadronic interaction between the CR protons and the ambient medium is multi-pion production (Blasi & Colafrancesco 1999):

$$\begin{aligned} p_{\text{CR}} + p_{\text{th}} &\Rightarrow \pi^0 + \pi^+ + \pi^- + \text{anything} \\ \pi^\pm &\Rightarrow \mu + \nu_\mu \\ \mu^\pm &\Rightarrow e^\pm + \nu_\mu + \nu_e \\ \pi^0 &\Rightarrow 2\gamma \end{aligned}$$

In this case the injection spectral rate of secondary e^\pm is (e.g. Brunetti & Blasi 2005):

$$\begin{aligned} Q_e(E) &= \int_{E_\pi} Q_\pi(E_\pi) dE_\pi \times \\ &\times \int dE_\mu F_e^\pm(E_\pi, E_\mu, E_e) F_\mu(E_\mu, E_\pi), \end{aligned} \quad (2)$$

where $F_e^\pm(E_e, E_\mu, E_\pi)$ is the spectrum of electrons and positrons from the decay of a muon of energy E_μ produced in the decay of a pion with energy E_π (taken from Blasi & Colafrancesco (1999), $F_\mu(E_\mu, E_\pi)$ is the muon spectrum generated by the decay of a pion of energy E_π (e.g. Moskalenko & Strong 1998), and the pion injection rate due to p-p collisions is (e.g. Dermer 1986; Blasi & Colafrancesco 1999; Brunetti & Blasi 2005)

$$\begin{aligned} Q_\pi(E_\pi) &= n_{\text{th}} c \int dE_p N(E_p) \beta_p F_\pi(E_\pi, E_p) \times \\ &\times \sigma_{pp}(E_p) \sqrt{1 - \left(\frac{m_p c^2}{E_p}\right)^2}, \end{aligned} \quad (3)$$

where n_{th} is the number density of thermal protons, σ_{pp} is the p-p cross-section, and F_π is the spectrum of pions from the collision between a CRp of energy E_p and thermal protons (e.g. Moskalenko & Strong 1998; Blasi & Colafrancesco 1999; Brunetti & Blasi 2005).

The observed synchrotron emission in radio halos at frequencies of \approx GHz requires energies of the secondary particles of several GeV, considering field strengths of \approx μ G typical of the IGM (e.g. Carilli & Taylor 2002). In this case a scaling model is appropriate to describe the pion-spectrum from p-p collisions, and we calculate $Q_e(E)$ from Eqs. 2–3 following Brunetti & Blasi (2005) and using a pion-spectrum :

$$F_\pi(E_\pi) = \frac{1}{2E_\pi} \left[c_1 \left(1 - \frac{E_\pi}{E_p}\right)^{3.5} + c_2 \exp\left(-18 \frac{E_\pi}{E_p}\right) \right] \quad (4)$$

where $c_1=1.22$ and $c_2=0.92$ (Berezinskii & Kudriavtsev 1990). The resulting electron source function can be approximated by :

$$Q_{e\pm}(E) = c n_{th} K_p E^{-\alpha_p} f(E, \alpha_p) \quad (5)$$

where $f(E, \alpha_p)$ accounts for the log-scaling of the p-p cross-section at high energies and causes the spectral shape to be slightly flatter than $E^{-\alpha_p}$; an analytical expression for the asymptotic form of f (for $E_\mu \gg m_\mu c^2$, $E_\pi \gg m_\pi c^2$, $E_p \gg m_p c^2$) is derived in Brunetti & Blasi (2005).

The steady state spectrum of high energy electrons in the IGM is given by (e.g. Dolag & Enßlin 2000):

$$N_e(E) = \left| \dot{E}(E) \right|^{-1} \int_E^\infty dE' Q_{e\pm}(E') \quad (6)$$

where the relevant cooling processes involve synchrotron and inverse Compton losses:

$$\dot{E}(E) = -\frac{4\sigma_T c}{3m_e^2 c^4} \left(\frac{B^2}{8\pi} + \frac{B_{CMB}^2}{8\pi} \right) E^2, \quad (7)$$

B is the local magnetic field strength and $B_{CMB}^2/8\pi$ gives the energy density of the CMB expressed as an equivalent magnetic field. We calculate the electron spectrum from Eqs. 2–4 and 6–7; this can be approximated by :

$$N_e(E) = \frac{6\pi m_e^2 c^4}{\sigma_T} n_{th} K_p E^{-(1+\alpha_p)} \frac{g(E, \alpha_p)}{B^2 + B_{CMB}^2} \quad (8)$$

where g is related to f in Eq. 5 via :

$$g(E, \alpha_p) = \frac{1}{E^{1-\alpha_p}} \int_E^\infty dX X^{-\alpha_p} f(X, \alpha_p) \propto E^\Delta \quad (9)$$

and $\Delta \approx 0.2$ for $E \approx$ few GeV.

The radio emissivity is :

$$j_\nu = \frac{\sqrt{3}e^3 B}{m_e c^2} \int_{E_{min}}^{E_{max}} \int_0^{\frac{\pi}{2}} dE_e d\theta \sin^2 \theta F\left(\frac{\nu}{\nu_c}\right) N_e(E) \quad (10)$$

where $\nu_c = (3/4\pi)p^2 e B \sin \theta / (mc)^3$ is the critical frequency and F the integral over the synchrotron kernel :

$$F(x) = x \int_x^\infty K_{\frac{5}{3}}(\xi) d\xi. \quad (11)$$

Here $K_{\frac{5}{3}}$ denotes the modified Bessel function of order 5/3.

For a power law spectrum of CRp, $N_p(E_p) \propto E_p^{-\alpha_p}$, the resulting synchrotron emission from secondary electrons is $j_\nu \propto \nu^{-(\alpha_p - \Delta)/2}$.

3.2 γ -rays from hadronic interactions

As already mentioned before, CRp - proton collisions produce neutral pions, which in turn decay to 2 photons. γ -rays are a direct measure of the CRp and provide a complementary constraint to the injection process of secondary electrons.

In order to allow for a prompt comparison with recent results we follow the formalism described in Pfrommer & Enßlin (2004) to estimate the γ -ray flux from CR in our simulations.

The γ -ray source function is :

$$q_\gamma(E_\gamma) \approx \frac{2^{4-\alpha_\gamma}}{3\alpha_\gamma} \frac{\sigma_{pp} c n_{th} K_p}{\alpha_p - 1} (E_{p,min})^{-\alpha_p} \frac{E_{p,min}}{\text{GeV}} \times \left(\frac{m_{\pi^0} c^2}{\text{GeV}} \right)^{\alpha_\gamma} \left[\left(\frac{2E_\gamma}{m_{\pi^0} c^2} \right)^{\delta_\gamma} + \left(\frac{2E_\gamma}{m_{\pi^0} c^2} \right)^{-\delta_\gamma} \right]^{-\alpha_\gamma/\delta_\gamma} \quad (12)$$

where $\alpha_\gamma \simeq \alpha_p$ is the asymptotic slope of the γ -ray spectrum, which resembles the slope of the proton spectrum (Dermer 1986). The shape parameter, which describes the semianalytic model near the pion threshold, is $\delta_\gamma = 0.14\alpha_\gamma^{-1.6} + 0.44$ by using an effective cross-section $\sigma_{pp} = 32 \times (0.96 + \exp(4.4 - 2.4\alpha_\gamma))$ mbarn. The integrated γ -ray source density λ_γ is then obtained by integrating the source function over energy (Pfrommer & Enßlin 2004) :

$$\lambda_\gamma = \int_{E_1}^{E_2} dE_\gamma q_\gamma(E_\gamma) = \frac{\sigma_{pp} m_\pi c^3}{3\alpha_\gamma \delta_\gamma} \frac{n_{th} K_p}{\alpha_p - 1} \frac{(E_{p,min})^{-\alpha_p}}{2^{\alpha_\gamma - 1}} \frac{E_{p,min}}{\text{GeV}} \left(\frac{m_{\pi^0} c^2}{\text{GeV}} \right)^{-\alpha_\gamma} \times \left[\mathcal{B}_x \left(\frac{\alpha_\gamma + 1}{2\delta_\gamma}, \frac{\alpha_\gamma - 1}{2\delta_\gamma} \right) \right]_{x_2}^{x_1} \quad (13)$$

where $\mathcal{B}_x(a, b)$ denotes the incomplete beta-function and $[f(x)]_a^b = f(a) - f(b)$.

3.3 The three models

To investigate the dependence of the predicted properties of non thermal emission of clusters on the underlying assumptions, we investigate 3 models for the distribution of magnetic fields and cosmic rays in clusters. They are chosen to encompass the reasonable range suggested by theoretical and observational findings.

We keep the spectral index fixed to $\alpha_p = 2.6$ in order to be able to match the typical spectrum of giant radio halos, $\alpha \sim 1.2 - 1.3$ (e.g. Ferrari et al. 2008), although a fraction of presently known halos has a steeper spectrum (e.g. Brunetti et al. 2008; Giovannini et al. 2009). Also, a spectral index $\alpha_p = 2.6$ allows to fit the spectral shape of the Coma halo at $\nu \leq 1.4$ GHz, although also in this case the spectrum steepens at higher frequencies (e.g. Thierbach et al. 2003; Donnert et al. 2010)

3.3.1 Model 1: Constant X_{CR}

In our first model the energy density of the CR protons is taken as a constant fraction of the thermal energy density. This is reasonable

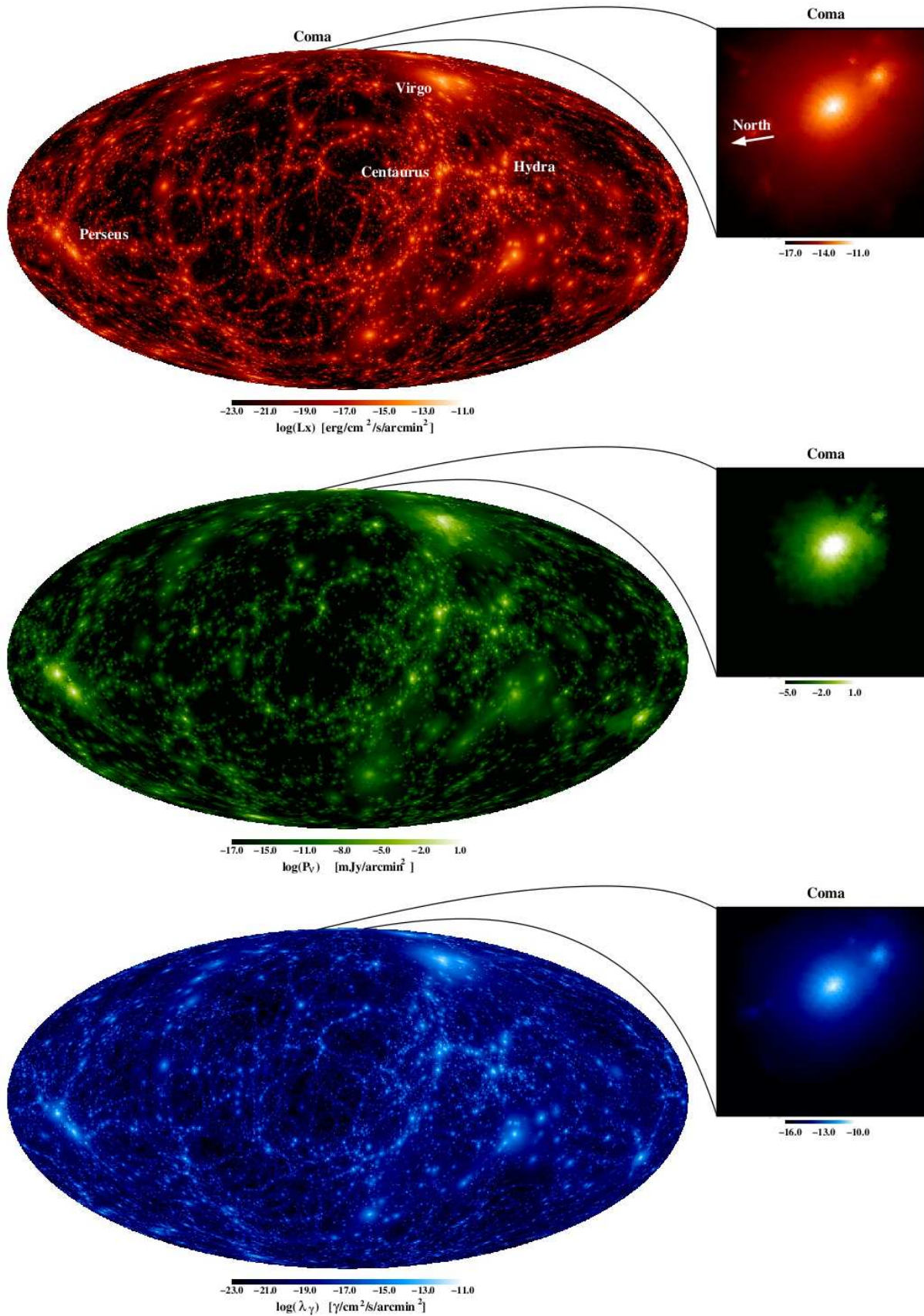


Figure 3. Full sky maps of the simulation in galactic coordinates. From top to bottom, X-ray, radio and γ -ray surface brightness are shown. For the radio and γ -ray emission the model with the constant cosmic ray energy fraction was chosen. The γ -ray emission is evaluated for VERITAS (e.g. $E > 100 \text{ GeV}$). The inlay shows a zoom onto a 3×3 degree region around the Coma cluster. In the upper most map, the most prominent clusters of the local universe are labeled and the arrow in the inlay points towards north.

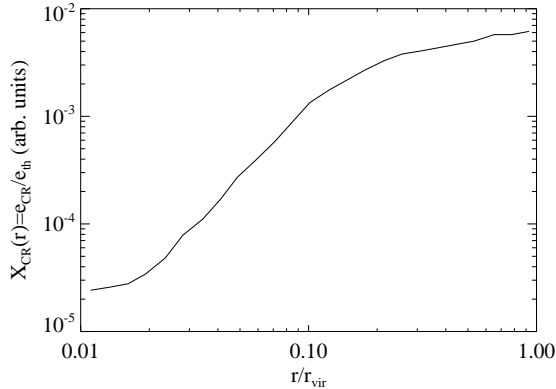


Figure 4. Energy in cosmic ray protons relative to thermal energy over cluster radius, inferred from Pfrommer et al. (2007). The dependence was derived assuming a linear relation between pressure and energy density.

if a constant fraction of the energy that is channeled into the IGM to heat the gas goes into the acceleration of CRp.

Therefore, in this model, the normalisation K_p is chosen to have a constant fraction, $X_p = \text{const}$, of kinetic CRp energy density ϵ_p to thermal energy density ϵ_{th} of the IGM:

$$\epsilon_p = X_p \epsilon_{th} \quad (14)$$

$$= \frac{K_p}{\alpha_p - 2} (E_{p,\min})^{2-\alpha_p} \quad (15)$$

For the magnetic field distribution within the IGM we take directly the magnetic field extracted from the simulations.

3.3.2 Model 2: Varying $X_{CR}(r)$

In a second model we adopt a radius dependent cosmic ray energy density fraction, $X_{CR}(r)$, as obtained from simulations of CR acceleration in structure formation shocks by Pfrommer et al. (2007). We also assume a constant CRp spectral index over the whole cluster volume, $\alpha_p = 2.6$.

Pfrommer et al. (2008) simulated the injection of CR protons by merger shocks during structure formation. They find that cosmic ray pressure increases relative to thermal pressure with increasing distance to the cluster centre. Assuming an ideal gas this directly translates into a radially increasing cosmic ray energy density fraction $X_{CR}(r) = \epsilon_{th}/\epsilon_p$. We use these results to infer a radially varying normalisation, so that Eq. 14 becomes:

$$\epsilon_p(\mathbf{r}) = X_p(r) \epsilon_{th}(\mathbf{r}) \quad (16)$$

$$= \frac{K_p(r)}{\alpha_p - 2} (E_{p,\min})^{2-\alpha_p}. \quad (17)$$

Figure 4 shows the radial dependence of the fraction used in agreement with the average over two cool core clusters, as shown in Pfrommer et al. (2008). The fraction increases by more than 2 orders of magnitude in the cluster external regions. This is expected to increase the extension of the diffuse radio emission generated by secondary electrons with respect to model 1. For the magnetic field distribution within the IGM we again use the magnetic field extracted from the simulations.

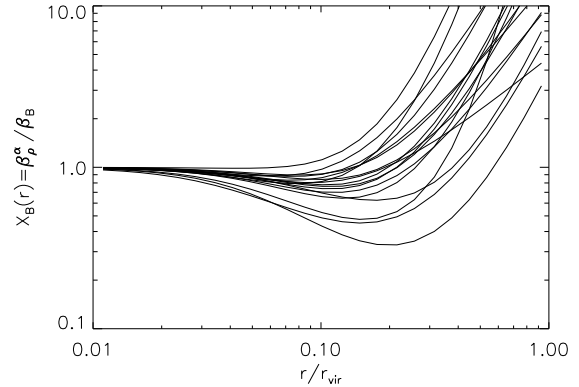


Figure 5. Scaling functions $f_{scal}(r)$ of all clusters. It modifies the magnetic field globally, so that its magnetic energy scales linear with thermal energy.

3.3.3 Model 3: Scaling $B \propto \sqrt{\rho}$

In our third model we modify the magnetic field originally obtained from the cosmological simulations.

The main reason for this is that the magnetic energy density, $\epsilon_{B,0}$, of the IGM is often modelled to follow thermal energy density, ϵ_{th} , which implies $B \propto \sqrt{\rho}$. In contrast to that we find $B \propto \rho$ in the outer regions of our simulated clusters. To allow a comparison with models that assume $B \propto \sqrt{\rho}$, we construct in our third model a function $f_{scal}(r)$ which scales the simulated magnetic field to follow $B \propto \sqrt{\rho}$ globally. This allows us to alter the dependence of the field with thermal density without losing its inherent structure which is a result of our simulations.

To construct the scaling function, we fit beta models $n_\beta = n_0(1 + r^2/r_{core}^2)^{3\beta/2}$ to spherically averaged density and magnetic field profiles. The scaling function is then:

$$f_{scal}(r) = \frac{(\rho_0(1 + r^2/r_{core,\rho}^2)^{3/2\beta_\rho})^{1/2}}{B_0(1 + r^2/r_{core,B}^2)^{3/2\beta_B}} \quad (18)$$

and is shown in figure 5 for every cluster in the sample. This changes the field strength at $r > 0.2R_{vir}$ without strongly affecting the field in the innermost regions.

For the cosmic ray distribution in this model, $X_p(r)$, we use the same radially dependent profile as in our model 2.

4 APPLICATION TO THE CLUSTER SAMPLE

Having the diffuse synchrotron emission from secondary electrons in our simulated clusters under control, the aim of this Section is to compare the simulated properties with the most relevant observational properties of radio halos.

We use an unprecedented sample of fairly-massive simulated clusters made by the 16 most massive objects extracted from our simulations. This allows for a statistical comparison with the main observational properties of radio halos obtained from studies of volume limited samples of radio halos in galaxy clusters. Additionally our sample (as well as the observational samples) contains the Coma cluster, so that we can calibrate K_p in all our models to match the observed radio luminosity of the Coma halo where needed.

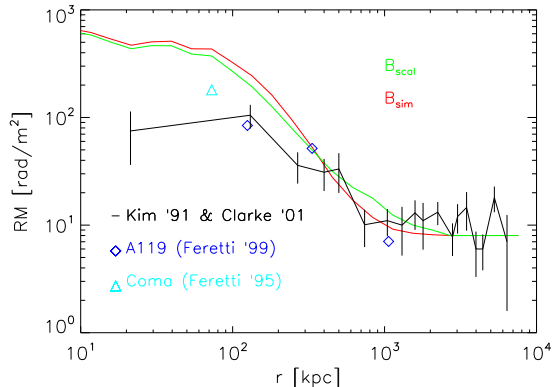


Figure 6. Faraday rotation over radius for a mass selected subsample of our simulated clusters. Shown are the original (green) and upscaled (red) median over the whole sample in every radial bin. We also plot observations from Coma (turquoise), A119 (blue) and a sample of Abell clusters (black) (Kim et al. 1991; Clarke et al. 2001; Feretti et al. 1995, 1999). The errors in Abell cluster sample were estimated using a bootstrapping technique (see text).

4.1 The magnetic field in our cluster set

The magnetic field obtained for our simulated Coma cluster is consistent with the one inferred from modeling Faraday Rotation Measures of the Coma cluster, as shown in (Donnert et al. 2010).

To compare the “statistical” properties of the magnetic field in the complete set of simulated clusters with observations and to show the effect of re-scaling the field (model 3), we plot in figure 6 radial profiles of Faraday Rotation. Here we bin all clusters with gas mass $M > 3 \times 10^{14} M_{\odot}$ in radius and take the median in each bin. In green we plot the field profile from simulations, and in red the scaled field profile (model 3). To compare we overplot observations of a sample of Abell clusters from Kim et al. (1991); Clarke et al. (2001), observations of A119 from Feretti et al. (1999) and observations of the Coma cluster (Feretti et al. 1995). Because of the small number of points, the error from the Abell clusters was estimated using a bootstrapping technique. For every bin we generate several samples, by selecting every data point a random number of times and computing the median of this subsample. We then compute the standard deviation of all samples to get an estimate of the error in each bin.

4.2 Radial profile of the radio emission

Since both the target thermal-protons and the expected magnetic field strength in the IGM decrease with distance from the cluster centre, most of the synchrotron luminosity emitted by secondary electrons should be produced in the cluster-core region. This causes the radial profile of secondary-generated radio halos to be substantially steeper than those of the observed halos (e.g. Brunetti et al. 2004), although formally this discrepancy may be alleviated by assuming that both the magnetic field and CRp have flat spatial distributions (Pfrommer & Enßlin 2004).

Cassano et al. (2007) report radial profiles of the radio emission of 5 well studied radio halos. We convolve our synthetic radio maps with a Gaussian using the typical beam size (43 kpc) of the observations, and in figure 7 compare these profiles with the observed ones. Both simulated and observed profiles were normalised to one.

We also include the radial profile of the Coma halo from Deiss et al. (1997).

In all cases (models 1–3), Figure 7 shows that the radial profiles of the secondary-generated radio halos in our simulated clusters are considerably steeper than the observed ones.

In agreement with Brunetti et al. (2004), by assuming a constant X_P (first panel), the simulated radio emission (black) for $r \geq 0.15R_{\text{vir}}$ is about 100 times below that measured in real radio halos (red, green).

By allowing X_P to increase with radius as in 3.3.2 results in an increase of the simulated emission for larger radii (figure 7, middle panel), but still expectations account for $< 10\%$ of the observed emission in real radio halos at $r \geq 0.15R_{\text{vir}}$. Additional up-scaling of the magnetic field (model 3) further increases the size of the simulated halos, especially at very large distances from the cluster center, where our MHD simulations would predict a steeper scaling of the magnetic field with gas density. However this up-scaling only mildly increases the level of the expected emission at intermediate distances, $r \approx 0.1 - 0.3R_{\text{vir}}$, where the radio brightness of radio halos is constrained by present observations.

In a recent paper Pfrommer et al. (2008) claim that, according to cosmological simulations, the combined synchrotron emission from secondary electrons and primary electrons accelerated at large scale shocks may produce diffuse emission with a fairly broad spatial distribution. Based on our results, the contribution from primary electrons (even assuming Pfrommer et al. (2008) results) is not expected to solve the discrepancy between models and observations in Fig. 7. Indeed, our model 3 is thought to mimic the secondary-generated emission in Pfrommer et al. (2008) and, based on their Figure 9, the contributions from primary electrons at $r \approx 0.2R_{\text{vir}}$ is (at best) comparable with that of the secondary electrons leaving expectations well below observations².

In principle, for each cluster, it would be possible to allow the energy density of CRp to further increase at large distances from the cluster center and find an *ad hoc* spatial distribution of CRp that allows for matching the brightness profiles of radio halos. However this would imply the untenable scenario in which CRp store very large energy budget outside the cluster core, for example in the case of the Coma halo the energy density of CRp at $r \approx 0.2 - 0.3R_{\text{vir}}$ should be comparable to that of the thermal ICM (Donnert et al. 2010).

4.3 Morphology of the radio emission

A complementary approach to compare expectations from simulations with observations is to derive a point-to-point plot between radio and X-ray brightness. A number of clusters indeed show morphological correlations between X-ray and radio surface brightness (Govoni et al. 2001). This could be preferable to a comparison of the radial profiles because morphological distortions and imperfect alignment of the emission centers may introduce errors in the observed profiles (Govoni et al. 2001).

In Figure 8 we show the luminosity in 166 kpc sized patches of our synthetic radio maps of the four biggest simulated clusters in

² it is more difficult to evaluate the ratio of secondary to primary electrons at $r \approx 0.3R_{\text{vir}}$ from Figure 9 in Pfrommer et al. due to the presence of a very bright shock-like spot southeast of the center of their simulated cluster (see their Figures 7 and 8) that affects the azimuthal brightness profile, but that is not indicative of an upturn in the distribution of the truly diffuse halo-emission

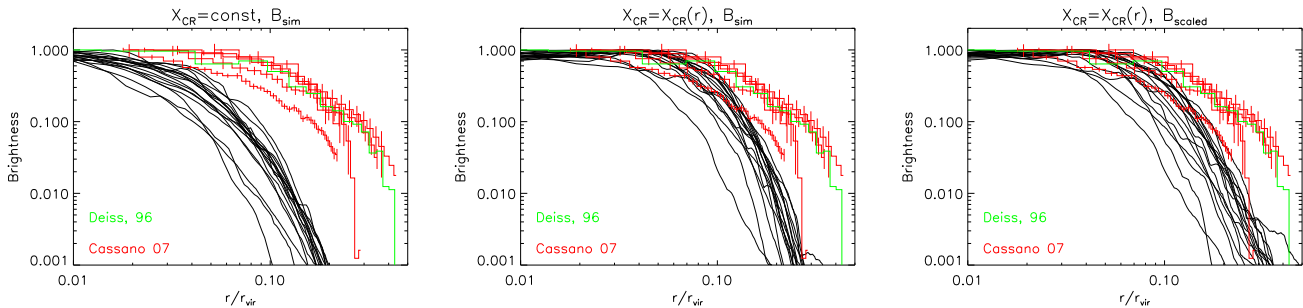


Figure 7. Normalized radial profiles of radio emission from 17 simulated clusters (black). In the left panel the CR population was modelled using a constant X_{CR} . The middle one uses the radius dependent CR to thermal energy fraction (fig. 4) adopted from Pfrommer et al. (2008). Additionally we modified (fig. 5) the magnetic field in the right panel to be $\propto \sqrt{\rho}$ (right panel). We add observations of A2744, A2319, A545, A2163 and A2255 from (Cassano et al. 2007) as red curves with error bars, Coma (green) is taken from Deiss et al. (1997).

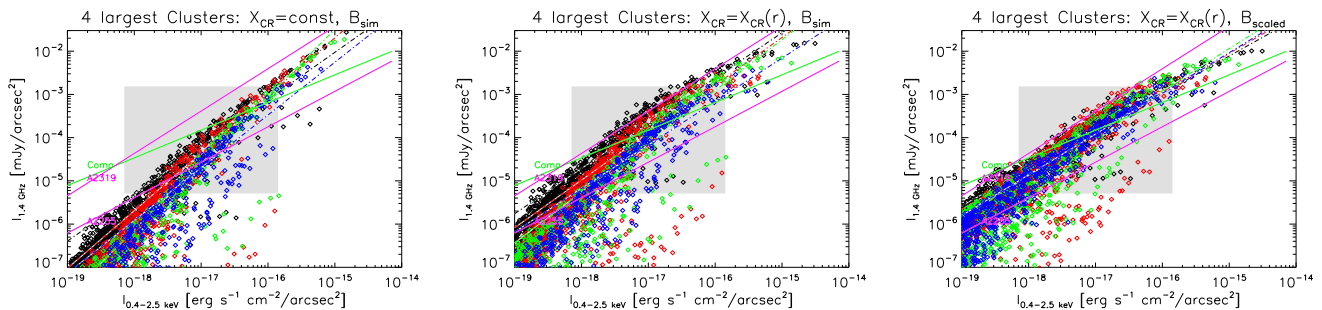


Figure 8. Radio vers. X-ray surface brightness in patches with 166 kpc side length, with the radio flux normalised to Coma. We also plot a fit to observations from Govoni et al. (2001) (red, $b = 0.64$ for COMA and A2255, A2319 dotted). The grey box indicates the observed region from Govoni et al. (2001).

Cluster	M1	M2	M3
0	1.09	1.04	0.87
PERSEUS	1.33	1.10	0.90
COMA	1.54	1.18	0.98
4	1.21	1.01	0.94

Table 2. Slopes of the Radio vers. X-ray surface brightness correlation from patches for our three models and the four largest clusters. Govoni et al. (2001); Feretti et al. (2001) find slopes of Coma & A2163: $b=0.64$, A2391: $b=0.98$ and, A2255: $b=0.82$

our sample as a function of the same patches in the X-rays. The three panels again show constant (model 1, left), increased cosmic ray scaling (model 2, middle) and cosmic rays scaled combined with magnetic fields scaled (model 3, right). We include the observed scaling for three clusters (A2255, Coma, A2319) from Govoni et al. (2001) (dashed lines) and add the correlations found from best fits to the simulated data (dashed dotted lines). In table 2 we include the slopes from a best fit model to the simulations inside the observed region. A comparison with the values found by Govoni et al. (2001); Feretti et al. (2001), (Coma, A2163: $b=0.64$, A2391: $b=0.98$, A2255: $b=0.82$) yields that only the third model may fit two of the three observations. Still no model approaches the flat value found for the Coma cluster.

We find that none of the models fit the slopes of any of the observed scalings over the whole range, with the radio brightness decreasing too quickly with respect to the X-ray brightness. This reflects the point raised in the previous Section, i.e. that the slope of the

radial distribution of the synchrotron emission in our secondary-generated radio halos is too steep.

In particular, the adoption of the cosmic ray scaling function (models 2 and 3) causes the emission to decrease in the innermost five patches, which can be seen in the plots as a bending at high brightness. The magnetic field scaling (model 3) adds more power to the outermost regions, resulting in a flattening of the correlation, but still the obtained slope is steeper than found in observations.

4.4 Scaling Relations

There are several observed correlations for radio halos that relate thermal and non-thermal properties of the IGM: those between the radio power at 1.4 GHz, $P_{1.4}$, and the X-ray luminosity, L_X , temperature, and cluster mass (Liang et al. 2000; Govoni et al. 2001; Cassano et al. 2006). In addition, by making use of a sample of 14 giant radio halos, Cassano et al. (2007) found new scaling relations that connect the radio power, P_R , of halos to the size of the emitting region, R_H (see also Murgia et al. 2009), and to the total cluster mass within R_H , M_H ; a geometrical scaling was also found between M_H and R_H . The observed scalings from Cassano et al. (2007) are :

$$P_R \propto R_H^{4.18 \pm 0.68} \quad (19)$$

$$P_R \propto M_H^{1.99 \pm 0.22} \quad (20)$$

$$M_H \propto R_H^{2.17 \pm 0.19} \quad (21)$$

Specifically, M_H was computed from X-ray observations under

the assumption of hydrostatic equilibrium and spherical symmetry. This procedure may lead to errors as large as 40% in mass (Rasia et al. 2006) which are expected to be not dependent on cluster mass, so that these errors might introduce considerable scatter without affecting the real trend of the correlation. R_H was measured on the radio images, $R_H = \sqrt{R_{\min} \times R_{\max}}$, where R_{\min} and R_{\max} are the minimum and maximum radii measured on the 3σ radio isophotes. We stress that R_H provides a simple, but viable estimate of the physical size of radio halos, indeed a one-to-one correlation has been found between R_H and the size containing the 85% of the radio halo flux, R_{85} , derived from the observed brightness profiles of halos (Cassano et al. 2007).

A scaling was also found between the size of radio halos and the virial radius of clusters, $R_H \propto R_{\text{vir}}^{2.63 \pm 0.50}$ (Cassano et al. 2007). Given that massive clusters are almost self similar (e.g. Rosati et al. 2002) one might have expected that R_H scales with R_{vir} and that the radial profiles of the radio emission are self-similar. On the contrary, this result proves that self-similarity is broken in the case of the non-thermal cluster components, as first noted by (Kempner & Sarazin 2001).

As the synchrotron power depends on both magnetic field scaling and CRe scaling with density, it is unclear what is responsible for the break in the observed properties. On the other hand we know from previous work (Donnert et al. 2008) that the magnetic field scaling (with temperature or mass) flattens out for the largest clusters in our simulation, that would imply an expected break of self similarity in the thermal vs non-thermal properties of our simulated clusters.

Cassano et al. (2007) showed that all the correlations explored so far for radio halos can be derived by combining the $R_H - R_v$ and $P_{1.4} - R_H$ scalings. This suggests that there are two main scaling relations that carry out the leading information on the physics of the non-thermal components in galaxy clusters.

In what follows we shall investigate whether the properties of our simulated secondary-radio halos are consistent with the observed scalings.

4.4.1 Mass vs. Size

As a first step, before comparing the observed scalings with those derived for our simulated clusters, we check whether our clusters inherit the same mass distribution of real clusters with radio halos. We compare the observed and simulated scaling between the total mass inside R_H (M_{85}) and R_{85} , that provides a geometrical scaling on the halo-region. Therefore we plot in Figure 9 M_H versus R_{85} for simulated (open triangles) and observed (diamonds) clusters, together with the best fit power law to the observed scaling from Cassano et al. (2007).

The three models define different values of R_{85} and consequently different volumes where the scaling can be tested. We find that in all cases simulated clusters lie on the thermal scaling described by observed clusters, although, as expected (Sects.4.2–4.3) simulations populate a region in the $M_H - R_{85}$ diagram with smaller values of R_{85} .

4.4.2 The Size vs. Size relation

As stated in Section 4.4, observations of clusters with radio halos show that the size of halos scales not linearly with the cluster virial radius, suggesting that the non-thermal component in clusters is not self-similar.

In figure 10 we plot the radius containing 85% of the clusters emission over virial radius for all three models. We include data from Cassano et al. (2007) and the fits to the simulated clusters-distribution obtained for models 1–3 at $z = 0$. We find a correlation between R_{85} and R_{vir} for our simulated hadronic-halos. Results suggest that self-similarity is preserved in the non-thermal components, as the increase of the halos’s radius is roughly proportional to the virial radius of the hosting clusters; the slopes of the correlations are $b_f = 0.8, 1.2$ and 1.3 for models 1, 2 and 3, respectively. This is not in line with observations: the expected correlations are flatter than the observed one and we predict halos systematically smaller than the observed ones. In contrast this is expected considering results reported in section 4.2 and confirms that it is challenging to reproduce the extension of the observed radio halos with hadronic models, even by adopting a profile of the magnetic field that is flatter than that from our MHD simulations and by assuming a flat profile of the spatial distribution of CRp (model 3).

Donnert et al. (2010) have shown that matching the radio emission of the Coma halo at distance $\approx 0.2 - 0.3 R_{\text{vir}}$ with hadronic models (by further increasing the CRp energy content at larger radii, see also section 4.2) would require the energy content of CRp to be roughly similar to the content of the thermal ICM at these distances (at least when constraints on the magnetic field from RM observations of the Coma cluster are used). The scalings found in figure 10 make the situation possibly more challenging, because they show that even more energy in the form of CRp would be required in the case of more massive clusters where the differences, between R_{85} of our hadronic-halos and that of the observed ones, are larger.

The observed clusters are in a range of redshifts, $z = 0 - 0.4$, while hadronic-halos are extracted from the simulations at $z = 0$. For this reason in figure 10a we also plot the distribution of simulated clusters obtained at $z = 0.4$ in the case of model 1 (marked green). We find that the correlation between $R_{85} - R_{\text{vir}}$ does not show significant change in slope at higher redshift.

4.4.3 The X-ray Luminosity vs. Radio power relation and the evolution of radio halos

Radio halos follow a correlation between the monochromatic radio luminosity at 1.4 GHz, $P_{1.4}$, and the X-ray luminosity of the hosting clusters, L_X (e.g. Liang et al. 2000; Enßlin & Röttgering 2002; Bacchi et al. 2003; Cassano et al. 2006). Recent radio observations of a statistical sample of X-ray selected galaxy clusters, the “GMRT radio halo survey”, (Venturi et al. 2007, 2008) allow to study the distribution of clusters in the $P_{1.4} - L_X$ diagram. These observations suggest that the distribution of clusters in the $P_{1.4} - L_X$ diagram is *bi-modal*: radio-halo clusters trace the $P_{1.4} - L_X$ correlation, while the majority of clusters are found “radio quiet” with the limits to their radio luminosities about 10 times smaller than the radio luminosities of halos.

In order to investigate the behaviour of our simulated clusters in the $P_{1.4} - L_X$ diagram, in Fig.11 we plot our simulated clusters together with observed clusters (from Venturi et al. (2008)). The synthetic radio luminosities of our simulated clusters are scaled in order to have the simulated Coma cluster matching the observed one.

According to secondary models a correlation between radio luminosity and cluster X-ray luminosity (or temperature) is expected (e.g. Dolag & Enßlin 2000; Miniati 2001; Dolag et al. 2005; Pfrommer et al. 2008). We qualitatively confirm these expectations and in all three models find that the largest simulated clusters would

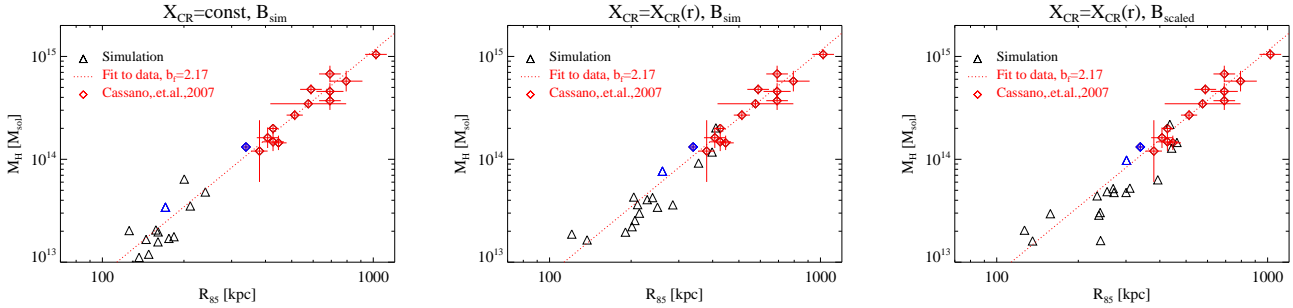


Figure 9. Total gravitational mass inside the radio emitting region over radius of the same region. We plot the correlation for all three models, constant and varying CR fraction and varying CR fraction and upscaled magnetic field (from left to right). We also plot observations of 14 galaxy clusters from (Cassano et al. 2007) and the best fit correlations. Due to uncertainties in the mass estimation from X-ray data the observations may show systematic errors. For both, simulations and observations the coma cluster is marked in blue.

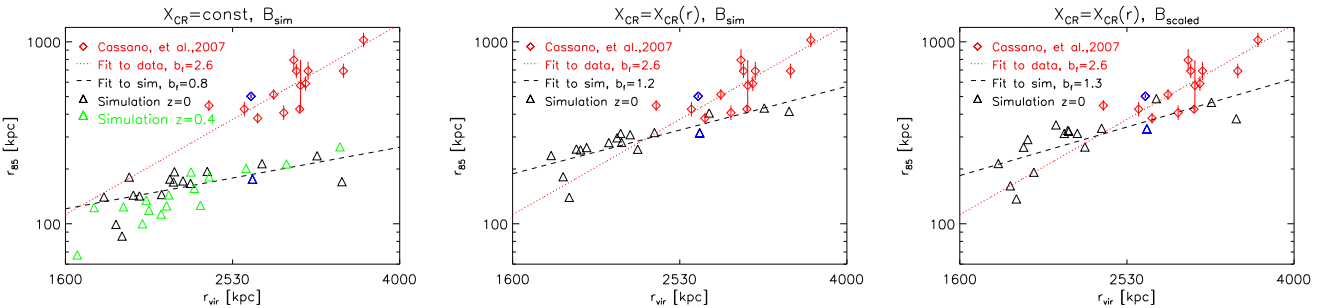


Figure 10. Radius of the radio emitting region as function of the virial radius of the cluster. We plot, left to right, the correlation for all three models and include the best fit ($\chi^2 = 0.54, 0.29, 0.86$, respectively). We also plot observations of 14 galaxy clusters from (Cassano et al. 2007) and the best fit correlation. For both, simulations and observations the Coma cluster is marked in blue. For model 1 we include the correlation at redshift 0.4.

naturally approach the observed correlation. In all three models the smallest systems are significantly more scattered in radio power than the largest clusters. This is expected as the magnetic field in the central regions of our simulated clusters (where most of the synchrotron emission is generated) is found to be tightly correlated with cluster thermal properties only in the case of massive clusters, while only a steep trend is found for smaller systems (figure 9 in Donnert et al. 2008).

The most relevant difference with respect to observations is that according to all three models (as for every secondary model) the synchrotron luminosity of the massive simulated clusters is equivalent to that of typical radio halos, at least if the radio luminosity of the simulated Coma cluster is normalised to that of the real Coma halo. This is inconsistent with observations which, on the other hand, found radio halos in only about 1/3 of massive clusters.

Most important, no radio *bi-modality* is expected in our simulated secondary-halos. Hadronic halos in simulated massive systems would follow a tight correlation, while those in less massive systems would be more broadly distributed.

One possibility to reconcile the hadronic scenario with the observed halo-merger connection and with the *bi-modal* distribution of clusters in the $P_{1.4} - L_X$ diagram is to admit that the observed *bi-modality* is driven by the amplification and dissipation of the magnetic field in the merging and post-merging phase, respectively (Brunetti & Lazarian 2007; Pfrommer et al. 2008; Kushnir et al. 2009). However, Burnetti et al. (2009) have shown that the degree of amplification/dissipation of the magnetic field and the time-scale of this process that would be necessary to explain observations are

difficult to reconcile with the observed properties of magnetic fields in the ICM (namely the field intensity and coherence scales from Rotation Measurements), and appear also disfavoured by energetic arguments.

The amplification of the magnetic field during cluster mergers is followed by our MHD cosmological simulations that offer a complementary approach to highlight this issue. To show the effect of magnetic field evolution and investigate the *bimodality* we plot the time evolution of the simulated radio haloes in figure 12. Shown is the radio luminosity over X-ray luminosity of the simulated sample for redshift $z < 0.48$ (big triangles: $z=0$, small triangles and black line: earlier redshifts); also we show the radio power vers. temperature correlation and evolution in the Appendix. No hint of a *bi-modality* is found, simply because magnetic field amplification in massive systems is a gradual process that happens in a time-scale comparable with the life-time of clusters themselves. The evolution of magnetic field is reflected in the broad/scattered distribution of clusters in the $P_{1.4} - L_X$ diagram, especially in the case of smaller systems. These smallest clusters approach the lower end of the correlation with rather large scatter because the magnetic field is not saturated yet in their central regions and even smaller mergers yield a significant field amplification resulting in an increased radio luminosity. Although one would expect this behavior to be slightly dependent on numerical resolution, increasing the numerical resolution would make the situation even more stringent. Resolving smaller gas motions leads to increase the amplification of the magnetic field, specially at early times. Having a larger magnetic field the changes in the magnetic field due to merger activity will be suppressed as the magnetic field is already closer to saturation effects.

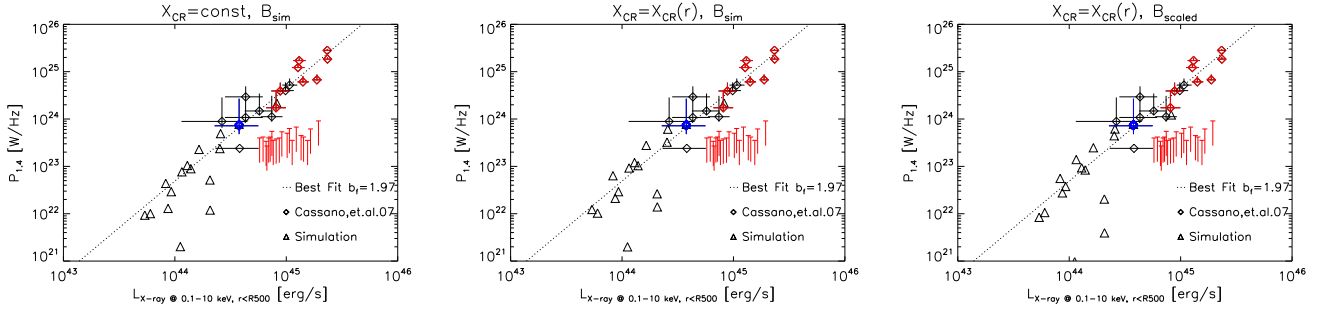


Figure 11. Radio power per frequency at 1.4 GHz over X-ray luminosity in erg/s from our simulated clusters using all three models (triangles, ltr.: constant fraction, scaled fraction, scaled fraction and scaled field). Observed scalings by Cassano et al. (2007) (diamonds, $z > 0.2$: red diamonds) and non-detections in red (Venturi et al. 2007, 2008). For both, simulations and observations the Coma cluster is marked blue.

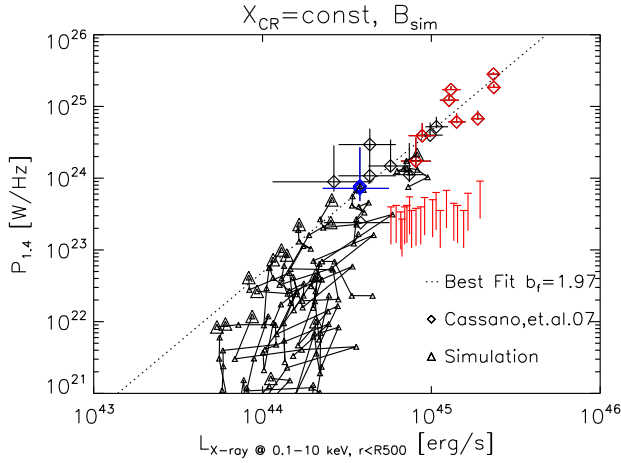


Figure 12. Radio power per frequency at 1.4 GHz over X-ray luminosity in erg/s from our simulated clusters using the constant model. Observed scalings by Cassano et al. (2007) (diamonds, $z > 0.2$: red diamonds) and non-detections in red (Venturi et al. 2007, 2008). We also include the time evolution of clusters for $z < 0.48$ (black lines)

Therefore we would expect the clusters (especially the smaller, less resolved systems) to evolve even more along the correlation, and the spread around it would be further decreased.

5 γ -RAY EMISSION FROM SIMULATED CLUSTERS

We use the formalism in section 3.2 to compute predictions for the γ -ray luminosity of the simulated clusters according to all three models. Of interest are the two energy bands of Cherenkov telescopes, $E > 0.1$ TeV, and FERMI/EGRET telescopes, $E > 0.1$ GeV.

In table 3 (4) we present fluxes for the simulated sample in the VERITAS (FERMI) energy band. None of the clusters is in the observable range of the VERITAS experiment, however the largest ones (0, Coma, Virgo, Perseus, Centaurus) have a chance to be detected by FERMI in next years, at least for models with radially increasing CRp normalisation (model 2 and 3).

In the left panel of figures 13 and 14 we plot the simulated clusters in γ -ray vers. radio luminosity at 1.4 GHz for the 3 models. Following the previous Section we normalise the radio luminosity of the sample so the simulated Coma cluster fits the

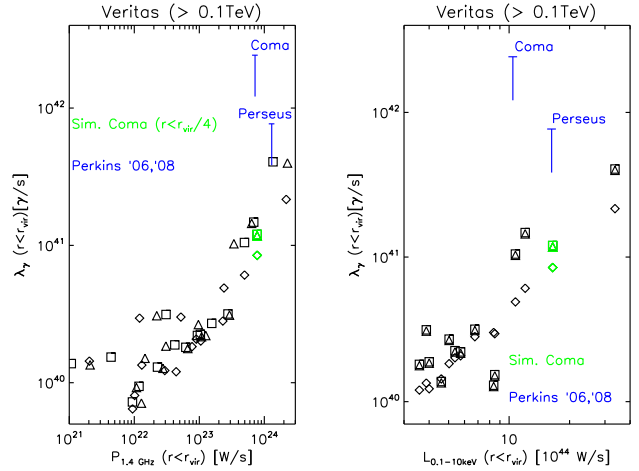


Figure 13. γ -ray luminosity ($E > 0.1$ TeV, e.g. VERITAS) over radio luminosity (at 1.4 GHz, left) and bolometric X-Ray luminosity of all cluster at redshift $z=0$. We plotted the three models as different symbols (diamonds - model 1, triangles - model 2, boxes - model 3) and include upper limits from Perkins (2008); Perkins & the VERITAS Collaboration (2006) in blue. The Coma cluster is marked green.

observed emission from the Coma halo. We also report available limits from VERITAS observations (Perkins 2008; Perkins & the VERITAS Collaboration 2006) (figure 13). Further we include (figure 14) newest preliminary results from the FERMI experiment (Mori 2009) on the upper limit of the γ -ray flux from the Coma cluster. A scaling between γ -ray and radio luminosity is expected for the 3 models because p-p collisions generate both secondary electrons and neutral pions, the scaling is sub-linear since the radio luminosity is further boosted by the increase of the magnetic field in more massive clusters.

In the right panel of figure 13 and 14 we plot the emission of our clusters in γ -ray vers. X-ray luminosity for the 3 models. Also in this case we show two γ -ray upper limits from VERITAS (Poullain et al. 1992) and preliminary FERMI (Mori 2009) observations respectively. A quasi-linear correlation is predicted, and is found less scattered than that between γ -ray and radio luminosities since it compares two purely thermal quantities (also in the case of models 2 and 3 CRp are scaled with thermal energy according with the profile in Figure 4).

The FERMI results are still consistent with the models for CRp pre-

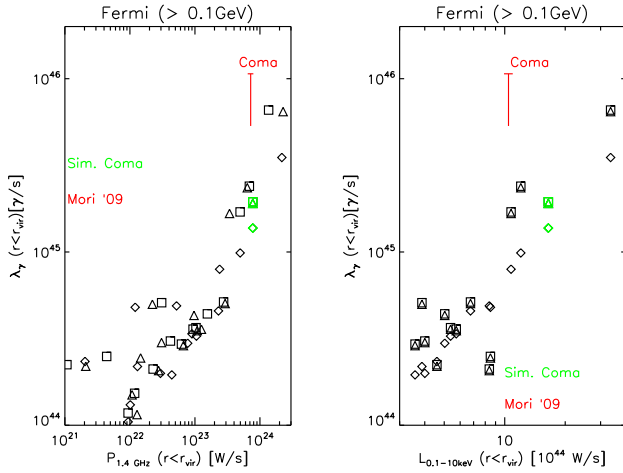


Figure 14. γ -ray luminosity ($E > 0.1\text{GeV}$, e.g. FERMI, EGRET) over radio luminosity (at 1.4 GHz, left) and bolometric X-Ray luminosity of all cluster at redshift $z=0$. We plotted the three models as different symbols (diamonds - model 1, triangles - model 2, boxes - model 3). We add preliminary results from the first year FERMI data (Mori 2009) in red. The Coma cluster is marked green.

Cluster	M1	M2	M3
0	3.2×10^{-13}	5.8×10^{-13}	6.0×10^{-13}
HYDRA	6.9×10^{-14}	3.3×10^{-14}	3.4×10^{-14}
2	2.4×10^{-14}	1.0×10^{-14}	1.0×10^{-14}
3	1.7×10^{-14}	2.5×10^{-14}	2.5×10^{-14}
4	9.9×10^{-14}	2.0×10^{-13}	2.1×10^{-13}
5	1.7×10^{-14}	2.6×10^{-14}	2.6×10^{-14}
COMA	6.7×10^{-14}	9.4×10^{-14}	9.6×10^{-14}
7	8.6×10^{-15}	9.8×10^{-15}	1.0×10^{-14}
8	1.8×10^{-14}	2.0×10^{-14}	2.1×10^{-14}
VIRGO	2.9×10^{-13}	6.7×10^{-13}	6.9×10^{-13}
A3627	3.2×10^{-14}	3.3×10^{-14}	3.4×10^{-14}
11	1.4×10^{-14}	2.1×10^{-14}	2.1×10^{-14}
12	4.5×10^{-14}	4.2×10^{-14}	4.3×10^{-14}
PERSEUS	9.7×10^{-14}	2.3×10^{-13}	2.3×10^{-13}
CENTAURUS	5.3×10^{-14}	5.8×10^{-14}	5.9×10^{-14}
15	5.0×10^{-15}	5.5×10^{-15}	5.6×10^{-15}

Table 3. Fluxes ($\gamma/\text{cm}^2/\text{s}$) in the VERITAS energy range ($E > 100\text{ GeV}$) from $1 R_{\text{vir}}$ for all Clusters from the simulations using the three different models.

sented in this paper. As shown by Donnert et al. (2010) the expected γ -ray flux increases substantially if we consider a spatial CR proton distribution so the radio emission actually fits the observations in morphology. We therefore expect a rejection or confirmation of our models in the very near future.

6 CONCLUSIONS

We use a constrained, cosmological MHD SPH simulation with a semianalytic model for galactic magnetic outflows, to obtain a sample of 16 galaxy clusters with thermal properties similar to clusters in the Local Universe. Further we assume 3 different models for secondary cosmic rays motivated by simulations (Pfrommer et al. 2007) using the proper high energy approximation for the pion cross-section. In the first model we assume a constant CRp

Cluster	M1	M2	M3
0	5.2×10^{-9}	9.5×10^{-9}	9.7×10^{-9}
HYDRA	1.1×10^{-9}	5.5×10^{-10}	5.6×10^{-10}
2	3.9×10^{-10}	1.6×10^{-10}	1.7×10^{-10}
3	2.8×10^{-10}	4.1×10^{-10}	4.1×10^{-10}
4	1.6×10^{-9}	3.4×10^{-9}	3.4×10^{-9}
5	2.8×10^{-10}	4.2×10^{-10}	4.3×10^{-10}
COMA	1.1×10^{-9}	1.5×10^{-9}	1.5×10^{-9}
7	1.4×10^{-10}	1.6×10^{-10}	1.6×10^{-10}
8	3.0×10^{-10}	3.3×10^{-10}	3.4×10^{-10}
VIRGO	4.7×10^{-9}	1.0×10^{-8}	1.1×10^{-8}
A3627	5.2×10^{-10}	5.4×10^{-10}	5.5×10^{-10}
11	2.3×10^{-10}	3.4×10^{-10}	3.5×10^{-10}
12	7.4×10^{-10}	6.9×10^{-10}	7.0×10^{-10}
PERSEUS	1.5×10^{-9}	3.7×10^{-9}	3.8×10^{-9}
CENTAURUS	8.7×10^{-10}	9.5×10^{-10}	9.7×10^{-10}
15	8.1×10^{-11}	9.0×10^{-11}	9.2×10^{-11}

Table 4. Fluxes ($\gamma/\text{cm}^2/\text{s}$) in the EGRET/FERMI energy range ($E > 0.1\text{ TeV}$) from $1 R_{\text{vir}}$ for all Clusters from the simulations using the three different models.

normalisation relative to the thermal density and the simulated magnetic field. In the second model we keep the magnetic field and introduce a radius dependent CRp normalisation inferred from non-radiative simulations by Pfrommer et al. (2007). The third model uses the same CRs and flatten the simulated magnetic field to be $B \propto \sqrt{\rho}$.

Although our simulations do not include a (internally) self-consistent treatment of CRp as done in other simulations (e.g. Pfrommer et al. 2007), contrary to previous work they allow to properly simulate the properties of the magnetic field in the ICM which is important for modeling the cluster-scale synchrotron emission.

For the first time, we carry out a detailed comparison between the observed properties of giant radio haloes and those of simulated halos according to secondary models and under different assumptions for the spatial distribution of CRp.

In an earlier paper we presented a detailed comparison of the simulated Coma cluster (Donnert et al. 2010). In this work we focus on global sample properties and compare with recent observations.

In particular, as a first step, we show that :

- The radial profiles of Faraday rotation of the median of our cluster sample is in line with that obtained from a number of observations of different clusters. This confirms that the properties of the clusters's magnetic fields in our simulations are rather similar to the observed ones.

- The normalised radial profiles of the radio emission at 1.4 GHz of our simulated hadronic-halos show a deficit at radii $\geq 0.1 r_{\text{vir}}$ with respect to the synchrotron profiles observed for a sample of well studied radio halos. This is in line with previous claims based on semi-analytic calculations in the context of the hadronic model (Brunetti et al. 2004). In addition our results show that, even by assuming a flat profile for both the magnetic field and CRp spatial distributions (Model 3), secondary electrons may account for less than about 10-15 % at radii 0.15 - 0.3 r_{vir} .

- A Point to Point comparison of radio vs. X-ray emission, obtained for the 4 largest clusters of our sample, confirms the results

obtained for the profiles showing that the radial distribution of radio emission is too steep. All three models do not fit the observations over the whole range. Furthermore an excess in radio emission of the innermost patches suggests that haloes from the simulation are to centrally peaked.

As a second step we compare scaling relations obtained for the hadronic-halos in our simulated cluster sample with those given in (Cassano et al. 2007) that are obtained from a sample of observed radio halos. We find that :

- The geometrical correlation between the radius of radio halos and the cluster-mass contained within this radius is well reproduced by all three models. Due to the expected self-similarity of cluster in thermal properties this result implies that -at least- the simulated and observed clusters share similar physical properties.
- A quasi self-similar behaviour is found for the non-thermal properties of our simulated clusters. In particular the radius of our hadronic halos is found to scale (approximately) with the virial radius of the simulated clusters. This is contrary to observations that found a steeper correlation between halo-radius and virial radius of the hosting clusters and implies that our simulated halos are systematically smaller than the observed ones.
- A correlation between the monochromatic luminosity of our hadronic halos and the X-ray luminosity of the simulated hosting-clusters is found. As soon as the population of our hadronic halos is normalised, by scaling the radio luminosity of the simulated Coma halo with that of the observed one, the correlation is similar to that observed for radio halos. However, since at this point all the simulated clusters show radio emission at the level of the observed halos, we find that the cluster radio *bi-modality*, observed for X-ray selected clusters, cannot be reproduced. A radio *bi-modality* in the radio – X-ray diagram would require a fast ($< \text{Gyr}$) evolution of the radio luminosity in connection with cluster mergers, on the other hand, we find that the time evolution of our simulated massive-clusters in this diagram happens on cosmological, long, time-scales. Finally, we show that once the radio – X-ray correlation is approached at low X-ray luminosities, clusters follow the correlation closely due to the saturation of the magnetic field.

As a final point we calculate the γ -ray emission from our simulated clusters once the radio luminosity of the simulated Coma halo is anchored to that of the observed one (essentially by scaling the number density of CRp in simulated clusters). We find that :

- The γ -ray emission expected from our simulated clusters is well below the sensitivity of present Cherenkov Arrays, e.g. the VERITAS experiment, for all the adopted models for hadronic halos. The γ -ray fluxes at $> 100 \text{ MeV}$ expected from our simulated clusters would allow for a marginal detection by the FERMI telescope in next years, at least by assuming Models 2 and 3.
- The integrated γ -ray flux from our simulated clusters is expected to scale with their radio emission, although with rather large scatter. On the other hand, a tight correlation is found between γ -ray and X-ray fluxes, in which case (due to the scalings between thermal and non-thermal CRp in Models 1–3) the correlation is essentially driven by the density of the thermal gas in our simulated clusters.

Considering all these results, as well as the outcome from our earlier work on the Coma cluster (Donnert et al. 2010), we conclude that hadronic models alone are not able to explain the observed properties of giant radio haloes, in terms of their radial extension, observed clusters’s radio *bi-modality*, scaling relations and

spectral properties. Therefore we conclude that radio emission observed in galaxy clusters in form of giant radio halos are a powerful tool to infer the amount of cosmic ray protons within galaxy cluster, confirming previous results that the energy content of cosmic ray protons in clusters can not exceed percent level (e.g. Brunetti et al. 2007; Churazov et al. 2008).

The problem of halo’s extension could be alleviated in *extended* hadronic models, where the contribution from primary (shock accelerated) electrons at the cluster outskirts is combined in the simulations with that from secondary electrons (Pfrommer et al. (2008)). However, as shown in Sect. 4.2, the problem of the halo profiles arises at distances $0.1 - 0.3 R_{\text{vir}}$ from cluster centers where, based on the same simulations, the contribution to the diffuse synchrotron emission from these shock accelerated electrons is not yet dominant. Further we would like to note that the detailed morphology of the radio emission caused by electrons injected at shocks (e.g. Roettiger et al. 1999)³ will be significantly different from the morphology of giant radio halos and therefore is in general unlikely able to mimic large scale, cluster centric radio emission. Thus additional physical processes are required to explain observations.

The problem of the radio *bi-modality* in massive clusters can be alleviated by assuming that MHD turbulence (and the rms magnetic field) decays as soon as clusters approach a relaxed state after a major merger (Brunetti et al. 2009; Kushnir et al. 2009). In this case it might also be thought that CRp in these relaxed clusters would undergo less scattering on magnetic field irregularities escaping from the cluster volume and reducing the source of secondary electrons. All these processes are not properly included in our MHD cosmological simulations. However, Brunetti et al. (2009) have shown that the fast decay of the rms field in galaxy clusters, that is necessary to explain the observed *bi-modality*, would imply a *rather unphysical* situation where the magnetic field power spectrum peaks at the smaller scales, and leads to the consequence that an *extremely* large flux of energy in clusters goes into magnetic field amplification/dissipation. In addition, because turbulent cascade should start to decay on largest scales, which are resolved by Faraday rotation measurements, this scenario would predict a *bi-modality* in rotation measures and depolarisation in largest clusters, which is not observed (Govoni et al. 2010).

The discovery of giant radio halos with *very* steep spectrum ($\alpha \sim 1.8 - 2$) in merging clusters proves that *inefficient* particle acceleration mechanisms are responsible for the origin of these sources and, based on simple energy arguments, disfavours hadronic models (Brunetti et al. 2008). Observations of the best studied halo, in the Coma cluster, have shown that its spectrum steepens at higher frequencies (Thierbach et al. 2003), due to the competition between energy losses and acceleration of the emitting particles, in which case the particle acceleration time-scale would be of the order of 0.1 Gyr. More recently we have shown that the steepening cannot be a result of the inverse Compton (SZ) decrement (Donnert et al. 2010), confirming these previous finding and supporting a scenario of *inefficient* particle acceleration mechanisms at the origin of the halo.

Particle acceleration due to micro-turbulence in merging galaxy clusters has been proposed for the origin of radio halos (e.g. Brunetti et al. 2001; Petrosian 2001). In this case *gentle* particle

³ These are base on Eulerian simulation, which are most appropriate to describe the morphology of shocks outside the cluster core.

acceleration mechanisms would generate radio halos in connection with (massive) cluster mergers, while the radio emission would decay as soon as clusters approach a relaxed state, due to dissipation of (at least a fraction of) this turbulence and the fast electron radiative cooling.

It will therefore be necessary to consider these processes in future simulations used to study radio halos. That includes an estimation of the locally merger injected turbulence as well as a more detailed description of CR electron spectra.

7 ACKNOWLEDGEMENTS

J. D. kindly acknowledges the support of ESF/Astrosim Exchange grant 2065 and thanks the INAF/IRA in Bologna for the hospitality. K. D. acknowledges the supported by the DFG Priority Programme 1177.

REFERENCES

- Aharonian F. e. a., 2009a, *A&A*, 502, 437
 Aharonian F. e. a., 2009b, *A&A*, 495, 27
 Bacchi M., Feretti L., Giovannini G., Govoni F., 2003, *A&A*, 400, 465
 Berezhinskii V. S., Kudriavtsev V. A., 1990, *ApJ*, 349, 620
 Berezhinsky V. S., Blasi P., Ptuskin V. S., 1997, *ApJ*, 487, 529
 Bertone S., Vogt C., Enßlin T., 2006, *MNRAS*, 370, 319
 Blasi P., 2001, *Astroparticle Physics*, 15, 223
 Blasi P., Colafrancesco S., 1999, *Astroparticle Physics*, 12, 169
 Borgani S., Dolag K., Murante G., Cheng L.-M., Springel V., Diaferio A., Moscardini L., Tormen G., Tornatore L., Tozzi P., 2006, *MNRAS*, 367, 1641
 Børve S., Omang M., Trulsen J., 2001, *ApJ*, 561, 82
 Brügggen M., Ruszkowski M., Simionescu A., Hoeft M., Dalla Vecchia C., 2005, *ApJ*, 631, L21
 Brunetti G., Blasi P., 2005, *MNRAS*, 363, 1173
 Brunetti G., Blasi P., Cassano R., Gabici S., 2004, *MNRAS*, 350, 1174
 Brunetti G., Cassano R., Dolag K., Setti G., 2009, *A&A*, 507, 661
 Brunetti G., Giacintucci S., Cassano R., Lane W., Dallacasa D., Venturi T., Kassim N. E., Setti G., Cotton W. D., Markevitch M., 2008, *Nature*, 455, 944
 Brunetti G., Lazarian A., 2007, *MNRAS*, 378, 245
 Brunetti G., Setti G., Feretti L., Giovannini G., 2001, *MNRAS*, 320, 365
 Brunetti G., Venturi T., Dallacasa D., Cassano R., Dolag K., Giacintucci S., Setti G., 2007, *ApJ*, 670, L5
 Buote D. A., 2001, *ApJ*, 553, L15
 Carilli C. L., Taylor G. B., 2002, *ARA&A*, 40, 319
 Cassano R., Brunetti G., 2005, *MNRAS*, 357, 1313
 Cassano R., Brunetti G., Rottgering H. J. A., Brügggen M., 2009, *ArXiv e-prints*
 Cassano R., Brunetti G., Setti G., 2006, *MNRAS*, 369, 1577
 Cassano R., Brunetti G., Setti G., Govoni F., Dolag K., 2007, *MNRAS*, 378, 1565
 Churazov E., Forman W., Vikhlinin A., Tremaine S., Gerhard O., Jones C., 2008, *MNRAS*, 388, 1062
 Clarke T. E., Kronberg P. P., Böhringer H., 2001, *ApJ*, 547, L111
 de Grijs R., 2001, *ArXiv Astrophysics e-prints*
 Deiss B. M., Reich W., Lesch H., Wielebinski R., 1997, *A&A*, 321, 55
 Dennison B., 1980, *ApJ*, 239, L93
 Dermer C. D., 1986, *A&A*, 157, 223
 Dolag K., Bartelmann M., Lesch H., 1999, *A&A*, 348, 351
 Dolag K., Bartelmann M., Lesch H., 2002, *A&A*, 387, 383
 Dolag K., Enßlin T. A., 2000, *A&A*, 362, 151
 Dolag K., Grasso D., Springel V., Tkachev I., 2005, *Journal of Cosmology and Astro-Particle Physics*, 1, 9
 Dolag K., Staszyszyn F. A., 2008, *ArXiv e-prints*, 807
 Donnert J., Dolag K., Brunetti G., Cassano R., Bonafede A., 2010, *MNRAS*, 401, 47
 Donnert J., Dolag K., Lesch H., Müller E., 2008, *ArXiv e-prints*, 808
 Dubois Y., Teyssier R., 2008, *A&A*, 482, L13
 Ensslin T. A., Biermann P. L., Klein U., Kohle S., 1998, *A&A*, 332, 395
 Enßlin T. A., Biermann P. L., Kronberg P. P., Wu X.-P., 1997, *ApJ*, 477, 560
 Enßlin T. A., Röttgering H., 2002, *A&A*, 396, 83
 Feretti L., 2003, *ArXiv Astrophysics e-prints*
 Feretti L., Dallacasa D., Giovannini G., Tagliani A., 1995, *A&A*, 302, 680
 Feretti L., Dallacasa D., Govoni F., Giovannini G., Taylor G. B., Klein U., 1999, *A&A*, 344, 472
 Feretti L., Fusco-Femiano R., Giovannini G., Govoni F., 2001, *A&A*, 373, 106
 Ferrari C., Govoni F., Schindler S., Bykov A. M., Rephaeli Y., 2008, *Space Science Reviews*, 134, 93
 Furlanetto S. R., Loeb A., 2001, *ApJ*, 556, 619
 Gabici S., Blasi P., 2003, *ApJ*, 583, 695
 Giovannini G., Bonafede A., Feretti L., Govoni F., Murgia M., Ferrari F., Monti G., 2009, *A&A*, 507, 1257
 Govoni F., Enßlin T. A., Feretti L., Giovannini G., 2001, *A&A*, 369, 441
 Grasso D., Rubinstein H. R., 2001, *Phys. Rept.*, 348, 163
 Hoffman Y., Ribak E., 1991, *ApJ*, 380, L5
 Kempner J. C., Sarazin C. L., 2001, *ApJ*, 548, 639
 Kim K.-T., Kronberg P. P., Tribble P. C., 1991, *ApJ*, 379, 80
 Klein U., Wielebinski R., Morsi H. W., 1988, *A&A*, 190, 41
 Kulsrud R. M., Cen R., Ostriker J. P., Ryu D., 1997, *ApJ*, 480, 481
 Kushnir D., Katz B., Waxman E., 2009, *Journal of Cosmology and Astro-Particle Physics*, 9, 24
 Li S., Li H., Cen R., 2008, *ApJS*, 174, 1
 Liang H., Hunstead R. W., Birkinshaw M., Andreani P., 2000, *ApJ*, 544, 686
 Mathis H., Lemson G., Springel V., Kauffmann G., White S. D. M., Eldar A., Dekel A., 2002, *MNRAS*, 333, 739
 Miniati F., 2001, *Computer Physics Communications*, 141, 17
 Miniati F., Jones T. W., Kang H., Ryu D., 2001, *ApJ*, 562, 233
 Mohr J. J., Mathiesen B., Evrard A. E., 1999, *ApJ*, 517, 627
 Mori M., 2009, *ArXiv e-prints*
 Moskalenko I. V., Strong A. W., 1998, *ApJ*, 493, 694
 Murgia M., Govoni F., Markevitch M., Feretti L., Giovannini G., Taylor G. B., Carretti E., 2009, *A&A*, 499, 679
 Perkins J. S., 2008, in *American Institute of Physics Conference Series Vol. 1085 of American Institute of Physics Conference Series, VERITAS Observations of the Coma Cluster of Galaxies*. pp 569–572
 Perkins J. S., the VERITAS Collaboration 2006, *ApJ*, 644, 148
 Petrosian V., 2001, *ApJ*, 557, 560
 Pfrommer C., Enßlin T. A., 2004, *A&A*, 413, 17
 Pfrommer C., Enßlin T. A., Springel V., 2008, *MNRAS*, 385, 1211

- Pfrommer C., Enßlin T. A., Springel V., Jubelgas M., Dolag K., 2007, MNRAS, 378, 385
- Pfrommer C., Springel V., Enßlin T. A., Jubelgas M., 2006, MNRAS, 367, 113
- Poullain P., Nieto J.-L., Davoust E., 1992, A&AS, 95, 129
- Pratt G. W., Croston J. H., Arnaud M., Boehringer H., 2008, ArXiv e-prints
- Rachen J. P., 2008, ArXiv e-prints, 808
- Rasia E., Ettori S., Moscardini L., Mazzotta P., Borgani S., Dolag K., Tormen G., Cheng L. M., Diaferio A., 2006, MNRAS, 369, 2013
- Reimer O., Pohl M., Sreekumar P., Mattox J. R., 2003, ApJ, 588, 155
- Roettiger K., Burns J. O., Stone J. M., 1999, ApJ, 518, 603
- Rosati P., Borgani S., Norman C., 2002, ARA&A, 40, 539
- Ryu D., Kang H., Biermann P. L., 1998, A&A, 335, 19
- Ryu D., Kang H., Cho J., Das S., 2008, Science, 320, 909
- Ryu D., Kang H., Hallman E., Jones T. W., 2003, ApJ, 593, 599
- Sarazin C. L., 1999, ArXiv Astrophysics e-prints
- Schlickeiser R., 2002, Cosmic Ray Astrophysics. Cosmic ray astrophysics / Reinhard Schlickeiser, Astronomy and Astrophysics Library; Physics and Astronomy Online Library. Berlin: Springer. ISBN 3-540-66465-3, 2002, XV + 519 pp.
- Springel V., 2005, MNRAS, 364, 1105
- Springel V., Hernquist L., 2002, MNRAS, 333, 649
- Subramanian K., Shukurov A., Haugen N. E. L., 2006, MNRAS, 366, 1437
- The MAGIC Collaboration Aleksić J. e. a., 2009, ArXiv e-prints
- Thierbach M., Klein U., Wielebinski R., 2003, A&A, 397, 53
- Völk H. J., Atoyan A. M., 2000, ApJ, 541, 88
- Vazza F., Brunetti G., Kritsuk A., Wagner R., Gheller C., Norman M., 2009, A&A, 504, 33
- Venturi T., Giacintucci S., Brunetti G., Cassano R., Bardelli S., Dallacasa D., Setti G., 2007, A&A, 463, 937
- Venturi T., Giacintucci S., Dallacasa D., Cassano R., Brunetti G., Bardelli S., Setti G., 2008, A&A, 484, 327
- Völk H. J., Aharonian F. A., Breitschwerdt D., 1996, Space Science Reviews, 75, 279

APPENDIX A: ADDITIONAL SCALING RELATIONS

Here we provide additional scaling relations to substantiate the scalings shown before.

A1 X-Ray luminosity - Temperature relation

In figure A1 we show bolometric X-ray luminosity over mass weighted temperature for the simulated cluster sample at redshift zero (diamonds) and 0.48 (triangles). We include band-corrected the observed relation from Pratt et al. (2008) (broken line) and a the same correlation normalised to the simulated Coma cluster (black line). It is well known that non radiative simulations tend to over predict the x-Ray luminosity by a fair amount (see for example (Borgani et al. 2006)). In addition the effect of K-correction can be seen in comparison with the cluster at high redshift.

Still, after re-normalizing the x-Ray luminosity there is a reasonably good agreement of with observations. We therefore conclude, that our simulated clusters sample shows similar thermal properties than the observations.

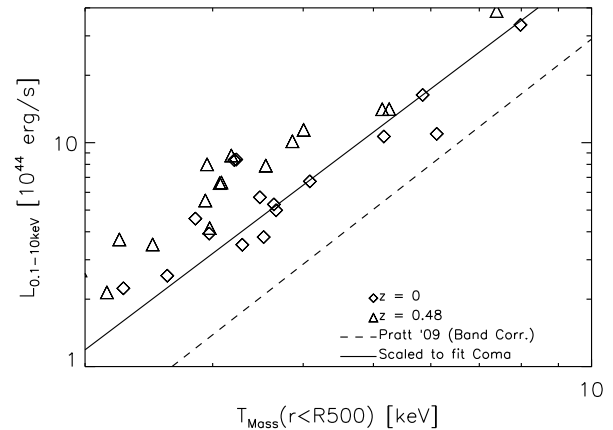


Figure A1. Bolometric X-Ray luminosity over temperature of all cluster at redshift $z=0$ (diamonds) and $z=0.48$ (triangles). We also plot the observed correlation from Pratt et al. (2008).

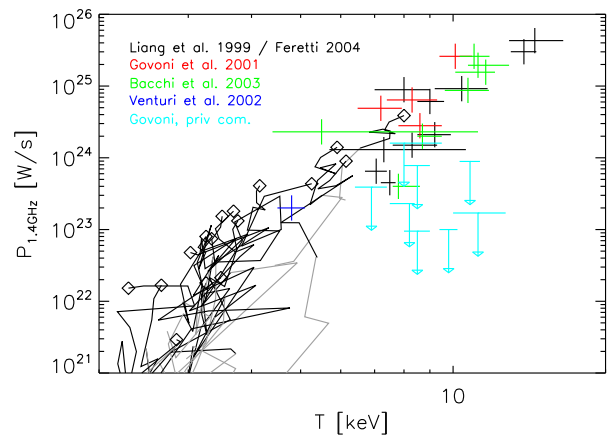


Figure A2. Radio Power at 1.4 GHz over mass weighted temperature inside $0.1r_{\text{vir}}$ for all clusters. We include various observations from the literature. The evolution of the simulated clusters is plotted as lines in black (gray) for $z < 0.48$ ($z > 0.48$), while the points correspond to $z = 0$.

A2 Radio luminosity - Temperature relation

In figure A2 we present the scaling of radio power at 1.4 GHz over cluster temperature as obtained from e.g. X-ray observations for constant CRp scaling (model 1). We include the evolution of the emission with time as lines in black (gray) for $z < 0.48$ ($z > 0.48$). Further we plot a number of recent observations. The sample follows the correlation closely at redshift zero, and only two clusters show significant deviation from the correlation at temperature larger than 5 keV, and only at high redshift.

In simulations, temperature is a less merger sensitive mass estimator compared to the X-ray luminosity, in terms of cluster mergers. We therefore conclude, that the bimodality observed in large clusters is not a result of biased mass estimation.